CellPress

Neuron
Article

Microtubule Minus-End Binding Protein CAMSAP2 Controls Axon Specification and Dendrite Development

Kah Wai Yau,[1,2] Sam F.B. van Beuningen,[1] Inês Cunha-Ferreira,[1] Bas M.C. Cloin,[1] Eljo Y. van Battum,[3] Lena Will,[1] Philipp Schätzle,[1] Roderick P. Tas,[1] Jaap van Krugten,[1] Eugene A. Katrukha,[1] Kai Jiang,[1] Phebe S. Wulf,[1] Marina Mikhaylova,[1] Martin Harterink,[1] R. Jeroen Pasterkamp,[3] Anna Akhmanova,[1] Lukas C. Kapitein,[1,*] and Casper C. Hoogenraad[1,2,*]

[1]Cell Biology, Faculty of Science, Utrecht University, 3584 CH, Utrecht, The Netherlands
[2]Department of Neuroscience, Erasmus Medical Center, 3015 GE Rotterdam, The Netherlands
[3]Department of Translational Neuroscience, Brain Center Rudolf Magnus, University Medical Center Utrecht, 3584 CG, Utrecht, The Netherlands
*Correspondence: l.kapitein@uu.nl (L.C.K.), c.hoogenraad@uu.nl (C.C.H.)
http://dx.doi.org/10.1016/j.neuron.2014.04.019

SUMMARY

In neurons, most microtubules are not associated with a central microtubule-organizing center (MTOC), and therefore, both the minus and plus-ends of these noncentrosomal microtubules are found throughout the cell. Microtubule plus-ends are well established as dynamic regulatory sites in numerous processes, but the role of microtubule minus-ends has remained poorly understood. Using live-cell imaging, high-resolution microscopy, and laser-based microsurgery techniques, we show that the CAMSAP/Nezha/Patronin family protein CAMSAP2 specifically localizes to noncentrosomal microtubule minus-ends and is required for proper microtubule organization in neurons. CAMSAP2 stabilizes noncentrosomal microtubules and is required for neuronal polarity, axon specification, and dendritic branch formation in vitro and in vivo. Furthermore, we found that noncentrosomal microtubules in dendrites are largely generated by γ-Tubulin-dependent nucleation. We propose a two-step model in which γ-Tubulin initiates the formation of noncentrosomal microtubules and CAMSAP2 stabilizes the free microtubule minus-ends in order to control neuronal polarity and development.

INTRODUCTION

Neurons are polarized cells that critically depend on the microtubule (MT) cytoskeleton for their development and function. Mutations in different Tubulin genes cause a range of nervous system abnormalities and several neurological and neurodegenerative diseases have been linked to altered MT-based transport processes (Franker and Hoogenraad, 2013; Millecamps and Julien, 2013). MTs, which serve as tracks for long-distance transport to axons and dendrites, are polarized structures with two distinct ends, the plus and minus-ends (Conde and Cáceres, 2009). Most plus-ends are highly dynamic, whereas minus-ends are believed to be much more stable. Control of MT plus-end dynamics, often by plus-end-associated proteins, has recently been shown to play an important role in determining neuronal polarity and in regulating dendritic spine morphology and synaptic plasticity (Jaworski et al., 2009). In contrast, little is known about the functions of neuronal MT minus-ends and potential minus-end-associated proteins.

In many cell types, most MT minus-ends are anchored and stabilized at a MT-organizing center (MTOC), most often the centrosome (Bettencourt-Dias and Glover, 2007). However, neuronal cells do not rely entirely on centrosomal MT nucleation. *Drosophila* neurons lacking an active centrosomes display a normal MT network and have proper axon outgrowth and neuronal organization (Basto et al., 2006; Nguyen et al., 2011). In addition, electron microscopy studies in sympathetic rat neurons show that most neuronal MTs are not anchored by the centrosome and do not form large radial arrays (Baas and Lin, 2011). More recent experiments found that during neuronal development, the centrosome loses its function as an MTOC (Stiess et al., 2010). Noncentrosomal MTs can be generated by two distinct mechanisms: severing of preexisting MTs or local nucleation at noncentrosomal sites, such as cortical γ-Tubulin complexes (Bartolini and Gundersen, 2006; Kuijpers and Hoogenraad, 2011; Stiess and Bradke, 2011). Depletion of the MT severing enzymes katanin and spastin was found to alter axonal growth in young neurons (Yu et al., 2008). MT nucleation at noncentrosomal sites has been reported to occur on Golgi membranes (Efimov et al., 2007). Additionally, a recent study in *Drosophila* neurons reports that Golgi outposts in dendrites locally nucleate MTs and shape dendrite morphology (Ori-McKenney et al., 2012).

Regardless of the precise mechanisms of noncentrosomal MT formation, in a sequential step the newly generated MT minus-end must be stabilized in order to prevent depolymerization (Bartolini and Gundersen, 2006; Dammermann et al., 2003). Recently, a MT minus-end binding protein, called Patronin, was found to protect MT minus-ends in *Drosophila* cells from

depolymerization (Goodwin and Vale, 2010). Three mammalian homologs of Patronin, calmodulin-regulated spectrin-associated protein 1–3 (CAMSAP1–3), have been identified (Baines et al., 2009). CAMSAP3/Nezha localizes at MT minus-ends close to adherent junctions in epithelial cells (Meng et al., 2008). Moreover, CAMSAP3/Nezha and CAMSAP2 cooperate in determining the overall growth pattern of MTs in epithelial cells (Tanaka et al., 2012), and recent in vitro experiments revealed that CAMSAP proteins associate with growing MT minus-ends and regulate their dynamics (Jiang et al., 2014). Nevertheless, whether these proteins also contribute to the establishment and maintenance of noncentrosomal MT arrays in developing and mature neurons has remained unresolved.

In this study, we use a combination of cell-biological approaches, quantitative/high-resolution microscopy, laser microsurgery, in utero electroporation, and organotypic slice cultures to determine the role of CAMSAP2 during neuronal polarity and development. We show that CAMSAP2 localizes to the MT minus-ends in axon and dendrites, stabilizes noncentrosomal MTs, and is required for axon specification, dendritic branch formation, and brain-derived neurotrophic factor (BDNF)-induced dendritic outgrowth. Together, these results reveal a new mechanism for stabilizing neuronal MTs and reveal a critical role for CAMSAP2 in axon specification and dendrite development.

RESULTS

Distinct CAMSAP2-Decorated Structures Are Present in Hippocampal Neurons

Little is known about the expression and distribution of the CAMSAP minus-end binding protein family in neurons. According to the in situ hybridization data from the Allen Mouse Brain Atlas and proteomics data set from the Human Protein Atlas project, CAMSAP2 is the most abundant family member in the hippocampus. Consistent with these data, western blot analysis of the three CAMSAP family members in the developing and mature hippocampus revealed that CAMSAP2 is the most abundant family member, whereas CAMSAP1 and CAMSAP3 could not be detected (Figure 1A). The CAMSAP2 antibody is specific for CAMSAP2, as it does not recognize the other CAMSAP family members (Figure 1B). Immunocytochemistry of mature hippocampal neurons at in vitro day 21 (DIV 21) with CAMSAP2 antibodies revealed a variety of small clusters and distinct (punctated) stretches, scattered throughout the cell body, axon, and dendritic shaft as revealed by the axonal marker Tau and dendritic marker MAP2 (Figure 1C). Similar results were obtained by immunostaining with two other CAMSAP2 antibodies and by low-level expression of GFP-tagged CAMSAP2 in neurons (Figure 1D; Figure S1 available online). CAMSAP2 stretches were found within the soma, axon, and dendritic shaft (Figures 1C and S1). CAMSAP2 was absent from the actin-rich dendritic spines, showed minimal overlap with the synaptic marker Bassoon (Figures 1F and S1), and lacked a significant degree of colocalization with the diffuse γ-Tubulin protein (Figures 1E and S2A).

Next, we analyzed endogenous CAMSAP2 in different stages of developing hippocampal neurons (from DIV 0–14) by immunostaining. The centrosome of young neurons (DIV 0–1), detected by immunostaining for Centrin or γ-Tubulin, did not overlap with CAMSAP2 (Figure S2B). Interestingly, the size of the CAMSAP2-decorated structures changed during neuron development: CAMSAP2-positive puncta ($\leq$1 μm) and small clusters (>1 μm and <10 μm) were clearly visible in young hippocampal neurons at <DIV 5 but less in mature cells, whereas long CAMSAP2 stretches ($\geq$10 μm) were abundantly present in mature neurons at >DIV 14 (Figures 1G and S2). The total CAMSAP2 expression levels were unchanged during neuronal development (Figure 1H). Thus, distinct CAMSAP2-decorated structures are present in hippocampal neurons, and the length of these structures changes during neuron development.

CAMSAP2 Localizes to MT Minus-Ends in Hippocampal Neurons

To further study the subcellular distribution of CAMSAP2, we performed *d*irect *st*ochastic *o*ptical *r*econstruction *m*icroscopy (dSTORM) imaging using neuron cultures stained for endogenous CAMSAP2 (Heilemann et al., 2008; Rust et al., 2006). In dSTORM reconstructions, CAMSAP2 stretches detected using conventional microscopy were often found composed of multiple shorter puncta or clusters of variable size (Figures 2A–2C). On average, 1.1 ± 0.3 CAMSAP2 puncta per μm^2 were observed in primary dendrites. To directly test whether CAMSAP2 localizes to MT ends in hippocampal neurons, we next optimized dSTORM imaging to resolve individual MTs within the crowded neuronal MT cytoskeleton. Whereas methanol fixation was required for immunolabeling of endogenous CAMSAP2, this was incompatible with sharp dSTORM imaging of MTs. In contrast, individual and continuous neuronal MTs, as well as many MT ends, could be clearly resolved using an optimized alternative fixation procedure that was compatible with GFP-based immunolabeling of GFP-CAMSAP2 (Figures 2D and 2E). Dual-color dSTORM imaging revealed that many individual MT ends were decorated with ~2–4 GFP-CAMSAP2 puncta, which appeared as stretches in diffraction-limited images (Figure 2F). Localization to MT ends was also observed with overexpressed GFP-CAMSAP3 in hippocampal neurons, except that the stretches were typically shorter and more continuous (Figure 2G). These data demonstrate that CAMSAP2 localizes to the ends of MTs in neurons.

To determine whether CAMSAP2 localizes to MT minus-ends, we expressed GFP-CAMSAP2 in COS7 cells together with mCherry-α-Tubulin and analyzed MT dynamics using TIRF microscopy. Consistent with previous observations (Tanaka et al., 2012), GFP-CAMSAP2 was specifically localized to one end of noncentrosomal MTs (Figure S3). The other end of these MTs alternated between rapid periods of growth and shrinkage, which is characteristic of MT plus-ends, suggesting that CAMSAP2 indeed enriches near the MT minus-end (Figure S3B; Movie S1). In addition, CAMSAP2 and the MT plus-end marker mCherry-MT+TIP were distributed differently along noncentrosomal MTs. The two proteins were localized at the opposite ends of the MT with the displacement of plus-end comets away from the GFP-CAMSAP2 signal (Figure S3C; Movie S2), demonstrating that CAMSAP2 localizes to MT minus-ends and allows MT extension and shortening by plus-end dynamics. Similar results were obtained in hippocampal neurons, where

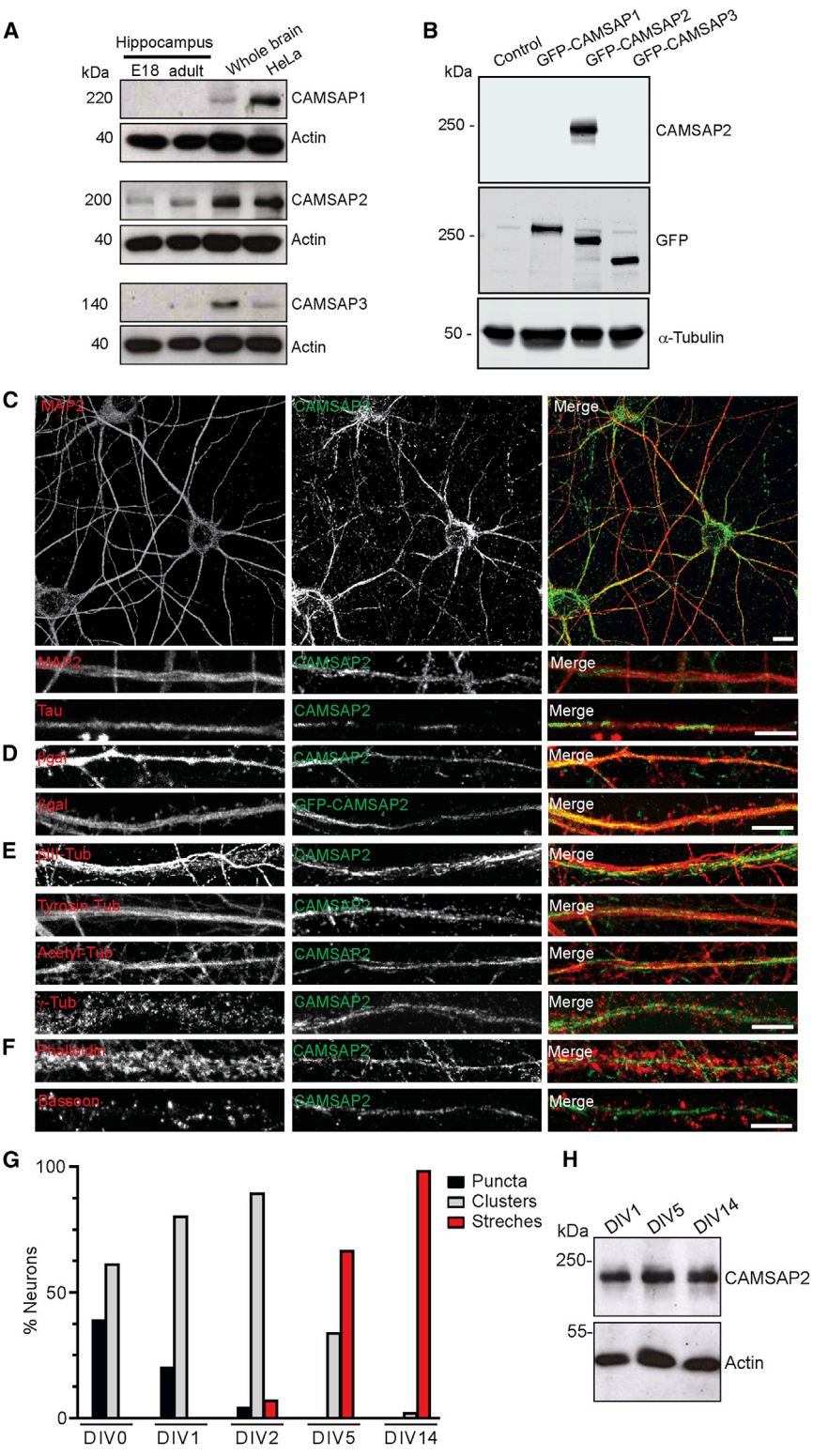

Figure 1. CAMSAP2 Distribution in Mature Hippocampal Neurons

(A) Extracts of whole hippocampus and brain of E18 embryos and adult rats were analyzed by western blot with indicated antibodies. HeLa cell extracts were used as a positive control.

(B) HEK293 human cells transiently expressing indicated GFP-CAMSAP proteins were analyzed by western blot with CAMSAP2 and GFP antibodies. α-Tubulin was used as a loading control.

(C) Representative confocal images of hippocampal neurons (DIV 21) stained for both endogenous MAP2 (red) or Tau (red) and CAMSAP2 (green). Dendritic segment is shown enlarged in the bottom row.

(D) Representative images of dendritic segments of hippocampal neuron (DIV 21) expressing β-galactosidase (red) to highlight neuronal morphology and either stained for endogenous CAMSAP2 (green, top) or cotransfected with GFP-CAMSAP2 (green, bottom).

(E and F) Double staining in hippocampal neurons (DIV21) for endogenous CAMSAP2 (green) with markers (red) for neuronal MTs (βIII-Tubulin), MT modifications (acetylated-Tubulin and tyrosinated-Tubulin), γ-Tubulin (E), actin (Phalloidin), and synapses (Bassoon) (F).

(G) Quantification of CAMSAP2 stretches throughout neuronal development. CAMSAP2 structures were divided into three categories: (1) puncta (approximately $\leq$1 μm), (2) clusters (approximately >1 μm and <10 μm), and (3) stretches (approximately $\geq$10 μm). At least 100 neurons were analyzed per developmental stage.

(H) Extracts of hippocampal neurons were prepared at the indicated time points and probed by western blot for CAMSAP2 and actin antibodies.

See also Figures S1 and S2.

GFP-CAMSAP2 specifically localizes to noncentrosomal MTs ends and MT plus-ends repeatedly emanated from stable CAMSAP2 stretches in the cell body (Figures 2H and 2I; Movie S3) and primary dendrites (Figures 2J and 2K; Movie S4). These results demonstrate that CAMSAP2 labels the minus-ends of noncentrosomal MTs in neurons.

Small CAMSAP2 Clusters Are Transformed to Extended Stretches

To characterize the dynamics of CAMSAP2-positive structures in primary dendrites of mature neurons, we examined the fluorescence recovery after photobleaching (FRAP) of GFP-CAMSAP2 stretches. On average, GFP-CAMSAP2 fluorescence recovered to 33% ± 1% of prebleached intensity after ~10 min with an average recovery half-time of 206 ± 20 s (Figure 3A). This recovery of CAMSAP2 is remarkably slow and incomplete when compared to the MT-associated protein MAP2, which recovered to 77% ± 1% of prebleached intensity after ~10 min with an average recovery half-time of 106 ± 6 s. Interestingly, while a small recovery was observed along the

length of the stretch, strong signals appear at the outmost edges of these structures (Figures 3B and 3C; Movie S5), suggesting that CAMSAP2 dynamics is increased at specific foci. To explore this phenomenon in more detail, GFP-CAMSAP2 recovery was monitored for extended periods (>30 min) in several stretches along the dendrite (Figures 3D–3F; Movie S6). CAMSAP2 stretches are highly dynamic along the dendritic shaft and recover as small clusters that typically grow from one side toward either the proximal or distal site of the dendrite (Figures 3E and 3F). The elongating CAMSAP2 stretches occasionally pause or shrink before continuing growing into longer stretches (Figures 3E and 3F). These results demonstrate that small CAMSAP2 clusters are transformed to extended stretches. This data suggest that, in neurons, MT minus-ends can slowly grow and be stabilized by accumulation of CAMSAP2, explaining the existence of very long stretches in older neurons.

CAMSAP2 Depletion Reduces MT Density in Neurons

To examine the function of CAMSAP2 in neuronal cells, we next used RNAi to suppress endogenous CAMSAP2 in developing (DIV 5) and mature (DIV 21) hippocampal neurons and analyzed the MT cytoskeleton. The efficiency of CAMSAP2 protein depletion was tested by introducing two independent CAMSAP2 shRNAs into neuronal cultures by lentiviral transduction. Western blot analysis revealed that both CAMSAP2 shRNAs reduced the levels of CAMSAP2 by ~85% (Figure 4A). Immunostaining experiments confirmed that CAMSAP2 intensity was strongly decreased in neurons expressing CAMSAP2 shRNA (Figures 4B and S4A–S4D). The level of polymerized MTs in neurons was analyzed by Tubulin preextraction, followed by measurement of endogenous MAP2 fluorescent staining intensity in CAMSAP2 shRNA-expressing neurons compared to the nontransfected neurons in the same field of view (Figure 4C). In DIV 5 neurons expressing CAMSAP2 shRNA, the MAP2 staining was reduced by ~80% compared to control cells (Figure 4E). This reduction greatly exceeded the effect of the potent MT-depolymerizing drug nocodazole (40% reduction; Figure 4F), suggesting that in the latter case the remaining MT network was stabilized by CAMSAP2.

In addition, the number of growing MT plus-ends was analyzed by immunostaining for endogenous EB3 upon knockdown of CAMSAP2. All control and shRNA expressing neurons showed the characteristic comet-like MT plus-end patterns (Jaworski et al., 2009), but the number of comets was markedly decreased in cells depleted of CAMSAP2 (Figure 4D). In young neurons at DIV 5, a decrease of ~30% of EB3 comets in axons, dendrites, and soma was found in CAMSAP2 shRNA-expressing neurons compared to control cells (Figure 4G). In mature neurons at DIV 21, the number of EB3 comets in the soma was only reduced by ~20% in CAMSAP2 knockdown cells (Figure 4H), while the number of comets in the primary and secondary dendrites was decreased by ~70% (Figures 4I and 4J). Live-cell imaging of EB3-GFP-labeled growing MT plus-ends confirmed these results: the number of EB3-GFP comets was decreased in CAMSAP2 knockdown neurons, but other parameters, such as the average growth velocity and the direction of displacement (retrograde versus anterograde), were not affected (data not shown). These data demonstrate that CAMSAP2 is important to establish and maintain the MT network in developing and mature neurons.

CAMSAP2 and γ-Tubulin Are Both Required for Noncentrosomal MTs

Because both CAMSAP2 and γ-Tubulin associate with MT minus-ends, we next investigated the relationship between γ-Tubulin and CAMSAP2 in neurons. We used RNAi to suppress endogenous γ-Tubulin in hippocampal neurons and analyzed the subcellular distribution and dynamics of CAMSAP2. Immunostaining experiments confirmed that γ-Tubulin was strongly downregulated in the cytoplasm of shRNA-expressing neurons (Figures S4E and S4F). Similar to the knockdown of CAMSAP2, the intensity of MAP2 and EB3 in γ-Tubulin-depleted neurons was markedly decreased (Figures 4E–4J), which is consistent with a role for γ-Tubulin in the nucleation of noncentrosomal MTs (Stiess et al., 2010). γ-Tubulin knockdown also reduced the intensity of CAMSAP2 by ~70% compared to control cells (Figures S4G and S4H). A similar decrease in CAMSAP2 staining was obtained by depleting two other subunits within the γ-Tubulin ring complex (γ-TuRC), γ-Tubulin complex-associated proteins GCP2 and GCP6 (Figures S4G and S4H). Importantly, simultaneous depletion of γ-Tubulin and CAMSAP2 showed no additive effect in the reduction of MT density (Figures 4E–4J), suggesting that the two proteins mostly operate in the same pathway.

To test whether GFP-CAMSAP2 localization to minus-ends directly depends on γ-Tubulin, we next used laser-based microsurgery to generate new MT ends (Figure 5A) and measure GFP-CAMSAP2 dynamics in control and γ-Tubulin-depleted cells. Upon laser-induced severing, GFP-CAMSAP2 was rapidly recruited to the newly generated MT minus-ends in both COS7 cells and neurons (Figures 5B–5G). Interestingly, repetitive MT plus-end growth and shrinkage was also observed from newly formed CAMSAP2 clusters (Figures 5B–5E; Movie S7), indicating that CAMSAP2 binding protects both sides of the decorated MT segments from depolymerization, consistent with in vitro observations (Jiang et al., 2014). The dynamics of GFP-CAMSAP2 accumulation upon laser-induced severing in γ-Tubulin knockdown neurons was indistinguishable from control cells (Figures 5F and 5G; Movie S8), indicating that CAMSAP2 can localize to MT minus-ends independent of γ-Tubulin. FRAP experiments with GFP-CAMSAP2 stretches in primary dendrites of γ-Tubulin knockdown neurons showed that although the number of events was reduced due to the decrease in overall MT density, the recovery rate and recovery levels were similar to the control cells (Figure 3A). The finding that γ-Tubulin depletion affects the number of CAMSAP2-decorated MT minus-ends but not the CAMSAP2 behavior is consistent with the in vitro data showing that CAMSAP family proteins accumulates on free, growing MT minus-ends, which are expected to lack γ-Tubulin (Goodwin and Vale, 2010; Jiang et al., 2014). Together, these data suggest that CAMSAP2 likely acts independently of γ-Tubulin at the molecular level but might act downstream after the generation of de novo noncentrosomal neuronal MT by γ-Tubulin.

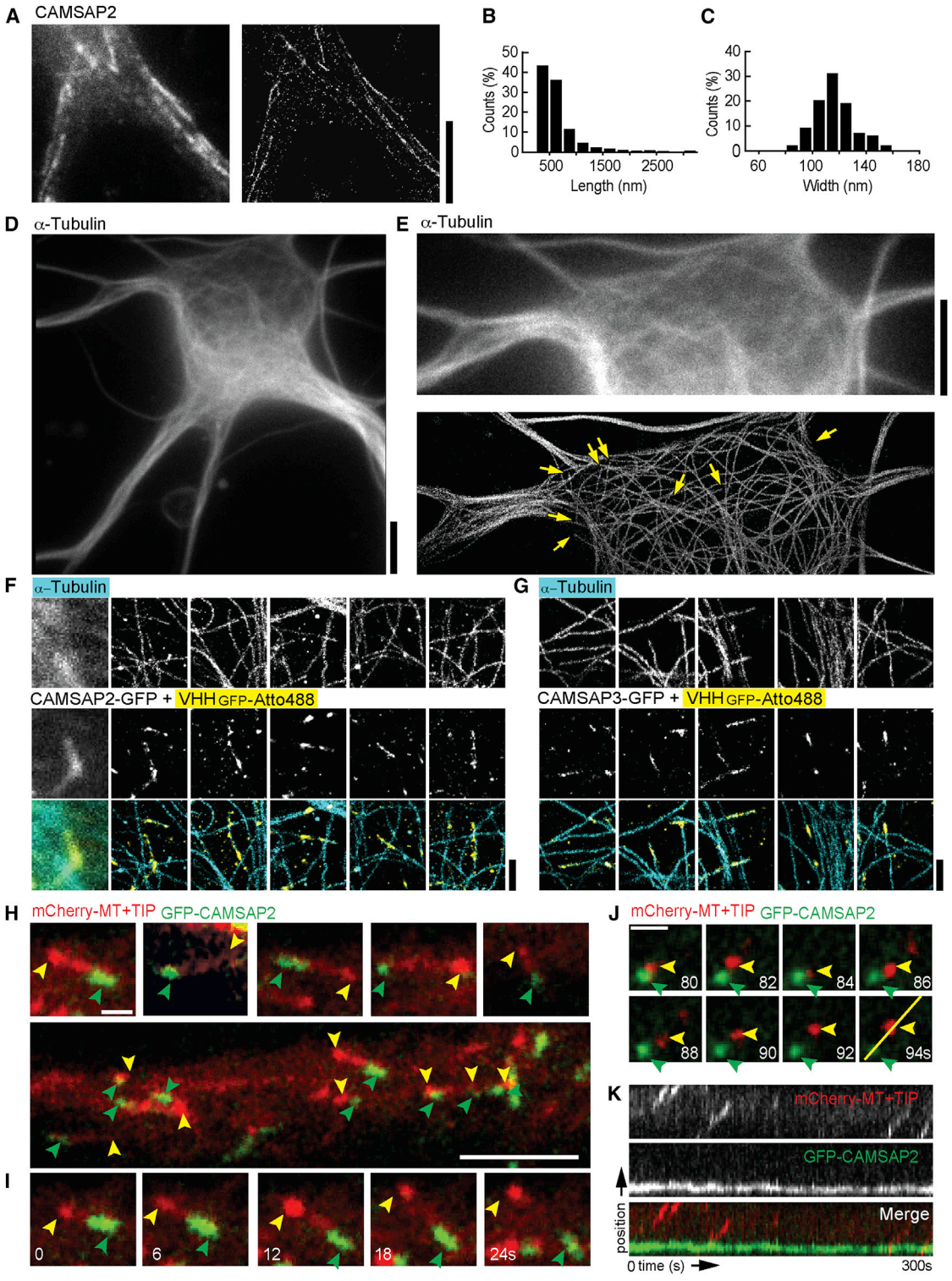

Figure 2. CAMSAP2 Localizes to Microtubule Minus-Ends in Hippocampal Neurons

(A) Conventional widefield image (left) and dSTORM reconstruction (right) of a methanol-fixed neuron stained for endogenous CAMSAP2 with Atto488. Scale bar is 5 μm.

(B) Distribution of stretch lengths including 316 stretches from seven neurons.

(C) Distribution of stretch widths (FWHM) based on Gaussian fitting (88 stretches from seven neurons).

(legend continued on next page)

CAMSAP2 Is Required for Dendrite Development and BDNF-Induced Dendritic Growth

Stable MTs are important for both dendrite development and maintenance (Conde and Cáceres, 2009). To determine whether CAMSAP2 controls normal dendrite morphology, we examined the effect of CAMSAP2 knockdown on dendrites in developing (DIV 5) and mature (DIV 20) hippocampal neurons using the two CAMSAP2 shRNAs. In both cases, we observed a marked change in dendrite morphology (Figures 6A and 6B). Dendritic length was decreased by ~30% in CAMSAP2 knockdown DIV 5 neurons compared to the control (Figure 6C). Moreover, knockdown of CAMSAP2 decreased the number of dendritic branches and total dendritic complexity, whereas the number of primary dendrites was not significantly changed (Figures 6C and 6D). A similar morphological phenotype was observed in mature neurons (Figures 6B, 6F, and 6G), indicating that CAMSAP2 is important for both dendritic development and maintenance. To obtain further insight in how CAMSAP2 regulates dendrite development, we determined whether the minimal CAMSAP2 domain required for minus-end binding (CC2-CC3-CKK, Figure S5) is sufficient to rescue the dendritic phenotype. Neurons were cotransfected at DIV 17 with CAMSAP2-shRNA and full-length GFP-CAMSAP2 or GFP-CC2-CC3-CKK for 4 days. This experiment showed that GFP-CAMSAP2 can restore the knockdown phenotype, while GFP-CC2-CC3-CKK expression was unable to rescue the CAMSAP2 phenotype (Figures 6K and 6L). These findings show that the minimal CAMSAP2 minus-end binding domain is not sufficient to restore dendrite morphology, suggesting that additional domains of CAMSAP2 are critical for CAMSAP2 function.

To further examine the role of CAMSAP2 in dendrite development, we compared the effect of BDNF in control and CAMSAP2 knockdown cells. BDNF causes dendritic growth in hippocampal neurons (Cheung et al., 2007). The control DIV 22 neurons cultured in the presence of 50 ng/ml BDNF for 3 days acquired ~41% additional dendrites (Figures 6I and 6J). In contrast, BDNF-induced dendrite formation did not occur in neurons expressing CAMSAP2 shRNA (Figures 6I and 6J). Together, these data demonstrate that CAMSAP2 is required for normal dendrite morphology and BDNF-induced dendritic growth.

Similar to knockdown of CAMSAP2, γ-Tubulin depletion also strongly reduced dendritic complexity in young and mature neurons (Figures 6E and 6H). Next, we tested whether CAMSAP2 acts upstream or downstream of γ-Tubulin in regulating dendrite morphology. While overexpression of GFP-CAMSAP2 partly restored the dendritic complexity in γ-Tubulin-depleted neurons (Figure 6N), GFP-γ-Tubulin expression was unable to rescue the CAMSAP2 phenotype (Figure 6M). These data suggest that CAMSAP2 expression is to some extent able to stabilize dendritic MTs and reverse the effects of γ-Tubulin knockdown. Together, these results demonstrate that CAMSAP2 and γ-Tubulin are important to maintain noncentrosomal MT arrays and dendrite morphology and that these factors might act sequentially: γ-Tubulin initiates the formation of de novo noncentrosomal MTs while CAMSAP2 stabilizes them.

Neuronal Activity Activation Affects the Distribution of CAMSAP2 in Dendrites

Previous studies have shown that neuronal activity modulates the stability of the MT arrays in dendrites (Halpain and Greengard, 1990). For instance, transient glutamate receptor activation suppresses MT growth and density (Kapitein et al., 2011). We next determined whether glutamate stimulation affects the distribution of CAMSAP2-decorated MT minus-ends in dendrites. Upon treatment with 50 μM glutamate for 5 min, the staining of CAMSAP2 stretches was markedly decreased and replaced by a more diffuse cytoplasmic signal within the dendrites, which could be blocked by the NMDA receptors antagonist APV (Figures S6A and S6B). In contrast, blocking either AMPA-type and kainate receptors (CNQX) or metabotropic glutamate receptors (AIDA) did not prevent the decrease in CAMSAP2 intensity at the dendrites (Figure S6B). We next determined whether a protocol to induce chemical LTD affects CAMSAP2 localization. Bath application of 50 μM NMDA for 5 min markedly decreased the intensity of the CAMSAP2-positive stretches in dendrites (Figures S6A and S6C). In mature hippocampal neuronal cultures, signaling through NMDA receptors mainly occurs through either NR2A- or NR2B-containing receptors. Using shRNA constructs that reduce the expression of NR2A and/or NR2B, we found that the knockdown of NR2B rather than NR2A blocked the NMDA-dependent CAMSAP2 redistribution (Figures S6A and S6C). Next we investigated GFP-CAMSAP2 dynamics upon NMDA stimulation. Consistent with the immunohistochemical data, NMDA stimulation induced a strong and rapid decrease in the intensity of the CAMSAP2-positive stretches in dendrites (Figure S6D). This effect started within the first minute after NMDA stimulation and persisted until GFP-CAMSAP2 signals fully disappeared, ~10 min after treatment (Figure S6E).

(D) Conventional widefield image of a DIV 5 neuron fixed using glutaraldehyde (GA) and paraformaldehyde (PFA) and stained with an AlexaFluor647-labeled antibody against α-Tubulin.

(E) Zoom of (D) (top) and corresponding dSTORM reconstruction (bottom), where multiple MT ends can be clearly observed. The final dSTORM image is a stitch of four partially overlapping reconstructions.

(F and G) Zooms from different DIV 5 neurons overexpressing CAMSAP2-GFP (F) or CAMSAP3-GFP (G), fixed with GA and PFA, and stained with an AlexaFluor647-labeled α-Tubulin antibody (top row) and a Atto488-labeled nanobody (VHH) against GFP (middle row). First two columns show conventional images and corresponding dSTORM reconstructions, followed by additional examples of CAMSAP2 decorated MT ends. Bottom row shows merge. Scale bars are 5 μm, except (F) and (G), which are 1 μm.

(H) Representative image of a dendritic segment from a hippocampal neuron (DIV 1) expressing mCherry-MT+TIP marker (red) and GFP-CAMSAP2 (green). Top row shows various examples. Yellow arrowheads indicate the MT plus-end; green arrowheads indicate the GFP-CAMSAP2-positive MT minus-end. Scale bars are 1 and 5 μm.

(I and J) Stills from TIRFM time-lapse recording of DIV 1 (I) and DIV 5 (J) neuron similar to (H). Scale bar is 1 μm.

(K) Kymograph of the yellow line (2.5 μm) shown in (J).

See also Figure S3 and Movies S1, S2, S3, and S4.

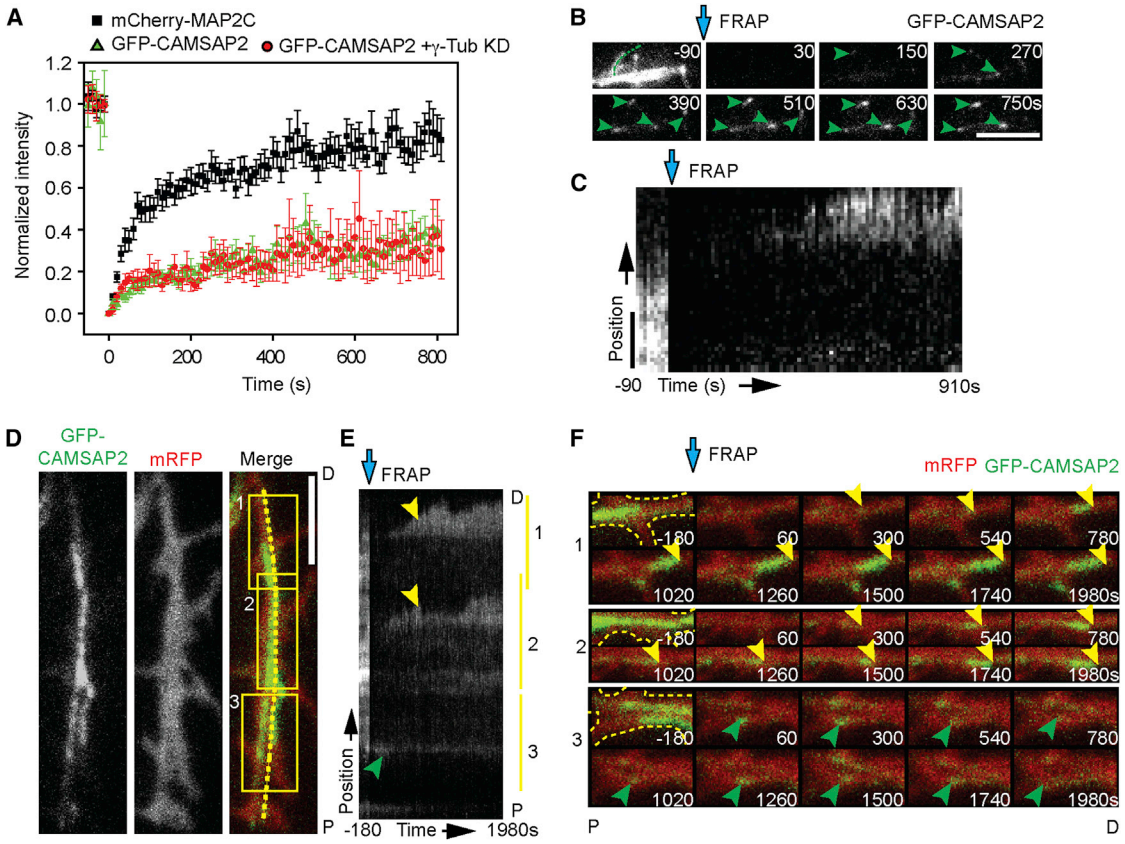

Figure 3. Elongating CAMSAP2 Clusters Form Extended Stretches in Neurons

(A) FRAP experiment intensity time traces of mCherry-MAP2C and pSuper (n = 12, black squares), GFP-CAMSAP2 and pSuper (n = 8, green triangles), or GFP-CAMSAP2 and γ-Tubulin shRNA (n = 5, red circles). FRAP was performed on GFP-CAMSAP2 stretches at t = 0. Error bars represent SEM.

(B) Stills from a TIRFM time-lapse recording of a neuron transfected with GFP-CAMSAP2. Green arrowheads point out recovery of specific points after photobleaching. Scale bar is 5 μm.

(C) Kymograph of a TIRFM time-lapse recording corresponding to the dashed green line in (B). Blue arrows indicates the FRAP (t = 0). Scale bar is 1 μm.

(D) Still frame from TIRFM time-lapse recording of a DIV 24 hippocampal neuron expressing mRFP (red) and GFP-CAMSAP2 (green). D indicates the distal end and P indicates the proximal end of the dendrite.

(E) Kymograph from the TIRFM time-lapse recording in (D). Green arrow heads indicate GFP-CAMSAP2 elongating toward the cell body; yellow arrowheads indicate GFP-CAMSAP2 growing away from the cell body.

(F) Still frames corresponding to the boxed regions of the TIRFM time-lapse recording in (D).

See also Movie S5 and S6.

Together, these data demonstrate that neuronal activity affects the distribution of CAMSAP2 in dendrites, which could explain the observed decrease in MT density after NMDA receptor stimulation (Kapitein et al., 2011).

CAMSAP2 Is Required for MT Stabilization during Neuronal Polarization

It is well known that the MT cytoskeleton is also important during early neuronal development, and changes in MT stability markedly affect neuronal polarity (Witte and Bradke, 2008). To investigate whether CAMSAP2 is directly involved in neuronal polarization, we first analyzed the distribution of endogenous CAMSAP2 in hippocampal neurons at early stages of development. Upon plating, hippocampal neurons first form lamellipodia around the cell body (stage 1) followed by the formation of several processes about 6 hr later, the minor neurites (stage 2). After 20–48 hr in culture, one neurite starts to grow out quickly and becomes the axon (stage 3), which can initially be labeled with the axonal marker Tau and later on with axon initial segment (AIS) markers, such as Ankyrin G, βIV-Spectrin, and sodium channels (pan-Nav). As reported previously (Stiess et al., 2010), distinct centrosomal components disappeared from the MTOC during neuronal development and dispersed throughout the cytoplasm at later stages (Figure S7), consistent with a shift from centrosomal to noncentrosomal nucleation. Indeed, dSTORM imaging revealed that, whereas in DIV1 cells many MTs emanated radially from the centrosome, DIV5 neurons had a nonastral MT organization with many free CAMSAP-decorated minus ends (Figures 2 and S6).

At 6 hr, all morphologically unpolarized neurons stained positively for endogenous CAMSAP2, showing puncta and small clusters in the soma and minor neurites (Figure 7A), and stained

negatively for axonal marker Tau and the earliest AIS marker Ankyrin G (Figures 7B and 7C). Thus, CAMSAP2 is already expressed in stage 2 cells before the neurons form an axon and polarize. At 24 hr, polarized neurons maintained CAMSAP2 expression within the soma, neurites, and Tau-positive axon (Figures 7A–7C). Interestingly, CAMSAP2 was present at low levels at the AIS region but enriched in the proximal part of the soma to the axon (Figure 7A). Closer inspection indicated that CAMSAP2 was abundant in the soma and in the first part of the axons, but not in the AIS, and was also present as small clusters and distinct stretches in the proximal axonal compartment directly after the AIS (Figure 7D). The high levels of CAMSAP2 at proximal part of the axon, right before the start of the AIS, was consistent across the neuronal population and maintained throughout neuronal development (Figures 7E and 7F).

To determine whether CAMSAP2 is involved in neuronal polarization, we knocked down CAMSAP2 before polarization in stage 1–2 neurons. Directly after dissection, primary cortical neurons were electroporated to deliver CAMSAP2 shRNA. At DIV 4, we determined the number of polarized neurons using the AIS marker pan-Nav and found a reduced fraction of polarized cells compared to control cells (Figure 7G), indicating that CAMSAP2 contributes to neuronal polarization. To further test whether CAMSAP2 plays a role in MT stabilization during axon initiation and specification, we used the MT-stabilizing drug taxol to induce multiple axon formation (Witte et al., 2008). In the presence of low concentrations of taxol (10 nM) for 2 days, the number of pan-Nav positive processes per cell was increased more than 3-fold in control neurons (Figure 7H). However, such taxol-induced axonal processes did not emerge in neurons expressing CAMSAP2 shRNA. The same phenotype was also observed after γ-Tubulin depletion (Figure 7H). Similar results were obtained by analyzing the axon-specific marker Tau and AIS marker βIV-Spectrin (Figures 7I and 7J). These in vitro data suggest that CAMSAP2 is required for axon specification.

CAMSAP2 Is Required for Axon Formation and Neuronal Polarity In Vivo

In the developing neocortex after terminal cell division, highly polarized neurons with a trailing process (future axon) and a unipolar leading process (future apical dendrite) are formed during neuronal migration (Barnes and Polleux, 2009). To investigate the effect of CAMSAP2 depletion in newborn neurons in the neocortex, we first performed ex vivo electroporation followed by organotypic slice cultures. E14.5 mouse embryos were subjected to intracranial electroporation to introduce GFP and CAMSAP2 shRNA plasmids selectively into neuronal precursors in the ventricular zone (VZ) (Figure 8A). Cortical slices were then prepared and cultured for 3 days to allow the labeled neurons to polarize and migrate to the cortical plate (CP) in a manner highly similar to that observed in vivo. Control GFP-positive neurons migrated to the CP (Figure 8B), while many CAMSAP2-depleted neurons accumulated in the (sub)ventricular zone (SVZ/VZ) and failed to migrate properly (Figure 8C), indicating that CAMSAP2 knockdown impairs neuronal migration in a cell-autonomous manner.

We next performed in utero electroporation for detailed analysis of neuronal morphogenesis. Following electroporation at E14.5, embryos were allowed to develop for 3 days (E17.5), at which point the morphology of GFP-positive migrating neurons was examined. In littermate controls, most GFP-positive migrating neurons possessed stereotypical bipolar morphologies consisting of a leading process and a long trailing-edge axon (Figure 8D). In contrast, cells expressing GFP and CAMSAP2 shRNA failed to form a distinguishable axon and the leading edge process (Figure 8E). Moreover, whereas GFP-positive axons projecting through the intermediate zone (IZ) were observed in control animals, such structures were not seen in CAMSAP2 shRNA-expressing animals (Figures 8D and 8E). In contrast, the radial glial cell fibers, expressing nestin, were not affected by CAMSAP2 shRNA expression (Figures 8F and 8G). Quantification revealed that ~80% of control neurons possessed a morphologically discernable leading process compared to ~30% of CAMSAP2-depleted cells (Figures 8H and 8I). Moreover, whereas ~70% of control cells in the IZ possessed axons, only ~20% of CAMSAP2 knockdown cells had discernible axons (Figures 8H and 8I). Together, these findings demonstrate that CAMSAP2 is critical for axon formation and the establishment of neuronal polarity in the developing neocortex.

DISCUSSION

Recent studies have identified different MT-mediated processes involved in regulating neuron polarization, development, and function (Conde and Cáceres, 2009; Hoogenraad and Bradke, 2009). MT minus-end dynamics has remained one of the least well-understood properties of the MT cytoskeleton in neurons. Especially, the mechanisms stabilizing the free noncentrosomal MT minus-ends have remained elusive. In this study, we demonstrate that by stabilizing minus-ends of noncentrosomal MTs, CAMSAP2 contributes to MT organization in developing and mature neurons, playing an important role in axon specification and dendritic branch formation in vitro and in vivo. In addition, similar to the widely used plus-end binding proteins to track growing MTs (Jaworski et al., 2009; Stepanova et al., 2003), the endogenous or fluorescently tagged CAMSAP2 provides a new molecular tool to identify noncentrosomal minus-ends and probe the MT organization in neuronal cells.

CAMSAP2 Stabilizes Noncentrosomal Minus-Ends in Neurons

Neuronal development and differentiation require sophisticated architectural changes, which may be incompatible with a large MT network emanating from a single MTOC (Kuijpers and Hoogenraad, 2011; Stiess and Bradke, 2011). Indeed, it has been shown that the centrosome loses its function as an MTOC during early neuronal development and that noncentrosomal MT arrays within axonal and dendritic processes acquire distinct organization patterns at later developmental stages (Baas et al., 1989; Stiess et al., 2010). In this study, we show that CAMSAP2 accumulates at neuronal MT minus-ends and plays a key role in stabilizing noncentrosomal MT arrays in axons and dendrites. We also found that small CAMSAP2 structures can grow and transform into extended stretches. The dynamic behavior of CAMSAP2 in neurons is likely explained by our recent data showing that CAMSAP proteins decorate growing MT minus-ends (Jiang

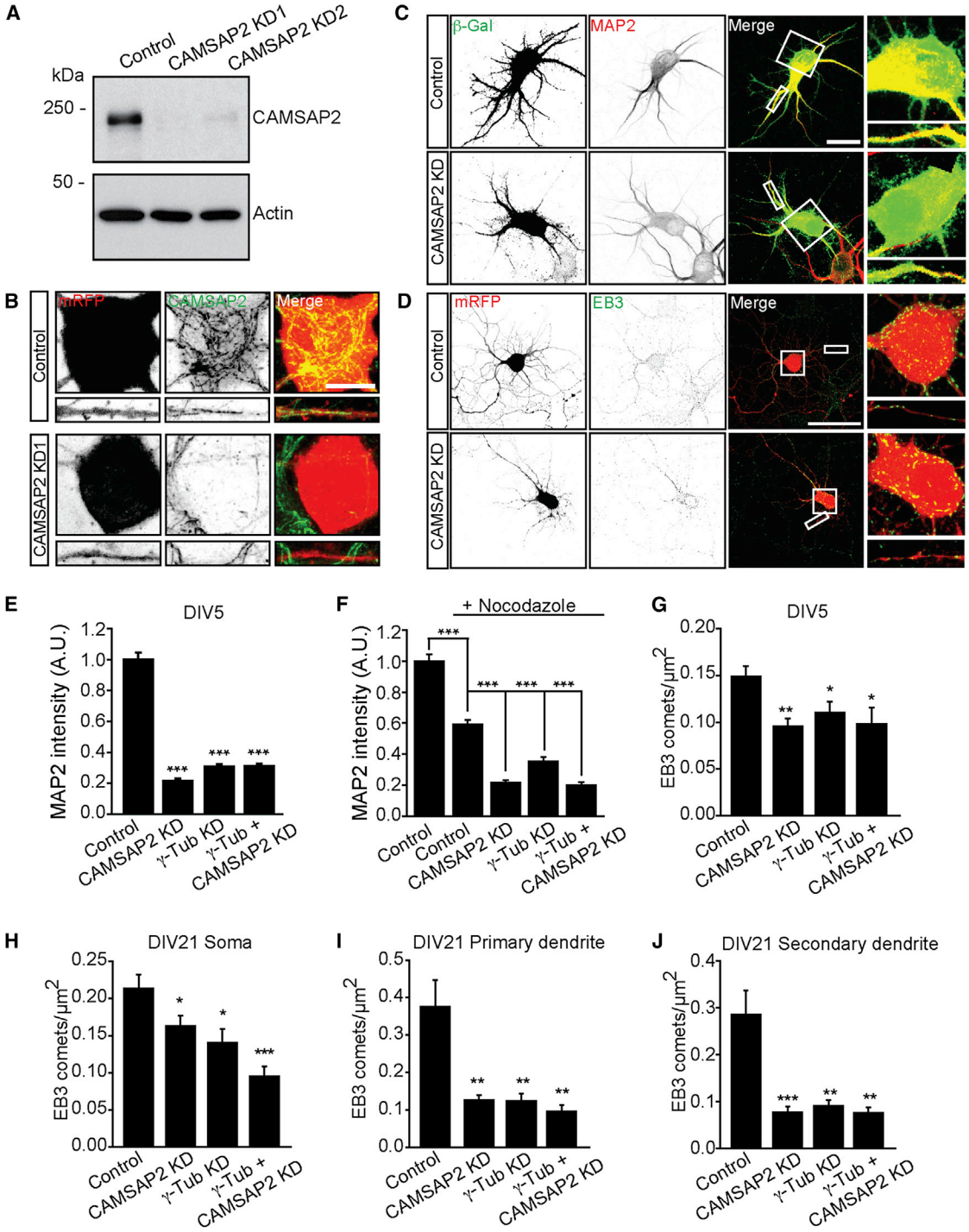

Figure 4. CAMSAP2 Stabilizes Microtubules in Neurons

(A) Extracts of DIV 25 hippocampal neurons sequentially infected at DIV 15 and DIV 20 with pSuper control, CAMSAP2-shRNA1 (KD1), and CAMSAP2-shRNA2 (KD2) lentivirus. Samples were analyzed by western blot with indicated antibodies.

(B) Representative images of hippocampal neurons transfected (DIV22) with mRFP (red) and pSuper (control) or CAMSAP2-shRNA1 (KD1) and stained for CAMSAP2 (green). Scale bar is 10 μm.

(C) Hippocampal neurons transfected at DIV 1 with β-galactosidase (green) and pSuper or CAMSAP2-shRNA, pre-extracted, fixed, and stained for MAP2 (red) at DIV 5. Scale bar is 20 μm.

(D) Hippocampal neurons at DIV 1 transfected with mRFP (red) and pSuper or CAMSAP2-shRNA, fixed, and stained for EB3 (green) at DIV 5. Scale bar is 50 μm.

(legend continued on next page)

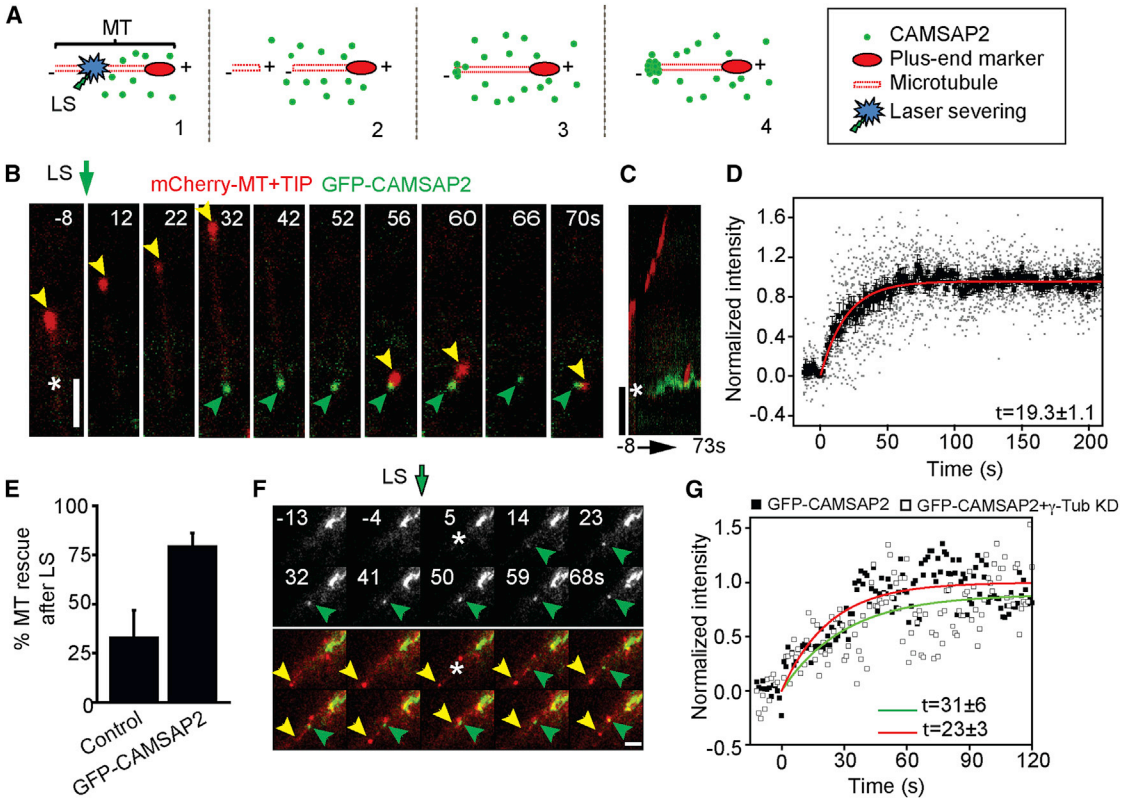

Figure 5. CAMSAP2 Can Localize to Microtubule Minus-Ends Independent of γ-Tubulin

(A) Schematic representation of MT laser-induced severing.

(B) Stills from a TIRFM time-lapse recording of a COS-7 cell expressing mCherry-MT+TIP (red) and GFP-CAMSAP2 (green). The yellow arrowheads indicate the MT plus-end marker. Green arrowheads indicate GFP-CAMSAP2 accumulating on MT minus-ends. Asterisk indicates the location of laser-induced severing at t = 0.

(C) Kymograph of the time-lapse recording shown in (B). Scale bars are 2 μm.

(D) GFP-CAMSAP2 intensity time trace of individual MT minus-ends (gray squares) and average trace (black squares) n = 10. Single exponential fit of the data average points is shown in red.

(E) Quantification of the percentage of MTs that are rescued after laser-induced severing after expression of GFP-CAMSAP2 (n = 4–6).

(F) Representative time-lapse recording of a hippocampal neuron (DIV 1) expressing GFP-CAMSAP2 (green) and mCherry-MT+TIP (red). Green arrowheads indicate GFP-CAMSAP2 accumulation, yellow arrowheads indicate MT plus-end, and the asterisk indicates the area of laser-induced severing. Scale bar is 1 μm.

(G) GFP-CAMSAP2 intensity time trace (black squares) of a TIRFM time-lapse recording; single exponential fit of the data points is shown in red. The white squares correspond to the intensity time trace of neurons transfected with GFP-CAMSAP2 and γ-Tubulin shRNA; single exponential fit of the data points is shown in green. Error bars represent SEM.

See also Movie S7 and S8.

et al., 2014). Although it is generally believed that MT minus-ends do not to grow (Dammermann et al., 2003), the numerous elongating CAMSAP2 stretches in various parts of the dendrites instead suggest that MT minus-end growth events frequently occur in hippocampal neurons. Since the length of the CAMSAP2 structures markedly changes during neuron differentiation, this might indicate that MT minus-end growth is developmentally regulated. Moreover, the need for MT minus-end

(E) Diagram showing the normalized mean intensity of MAP2 in dendritic regions from DIV 5 neurons expressing control pSuper (n = 26), CAMSAP2-shRNA (n = 23), γ-Tubulin-shRNA (n = 20), or both CAMSAP2-shRNA and γ-Tubulin-shRNA (n = 20). AU, arbitrary unit.

(F) Diagram showing the normalized mean intensity of MAP2 in dendritic regions from neurons, which have been untreated (n = 26) or treated with 30 μM nocodazole transfected as in (E) (n = 19, n = 15, n = 13, and n = 15, respectively). AU, arbitrary unit.

(G) Diagram showing the average number of EB3 comets/μm^2 in DIV 5 neurites transfected as in (E) at DIV 1 (n = 11, n = 11, n = 11, and n = 12, respectively).

(H) Diagram showing the average number of EB3 comets/μm^2 in DIV 21 soma transfected as in (E) at DIV 17 (n = 16, n = 19, n = 10, and n = 12, respectively).

(I) Diagram showing the average number of EB3 comets/μm^2 in DIV 21 primary dendrites transfected as in (E) at DIV 17 (n = 16, n = 19, n = 10, and n = 12, respectively).

(J) Diagram showing the average number of EB3 comets/μm^2 in DIV 21 secondary dendrites transfected as in (E) (n = 16, n = 19, n = 10, and n = 12, respectively).

Error bars represent SEM. *p < 0.05; **p < 0.01; ***p < 0.001 (t test).

See also Figure S4.

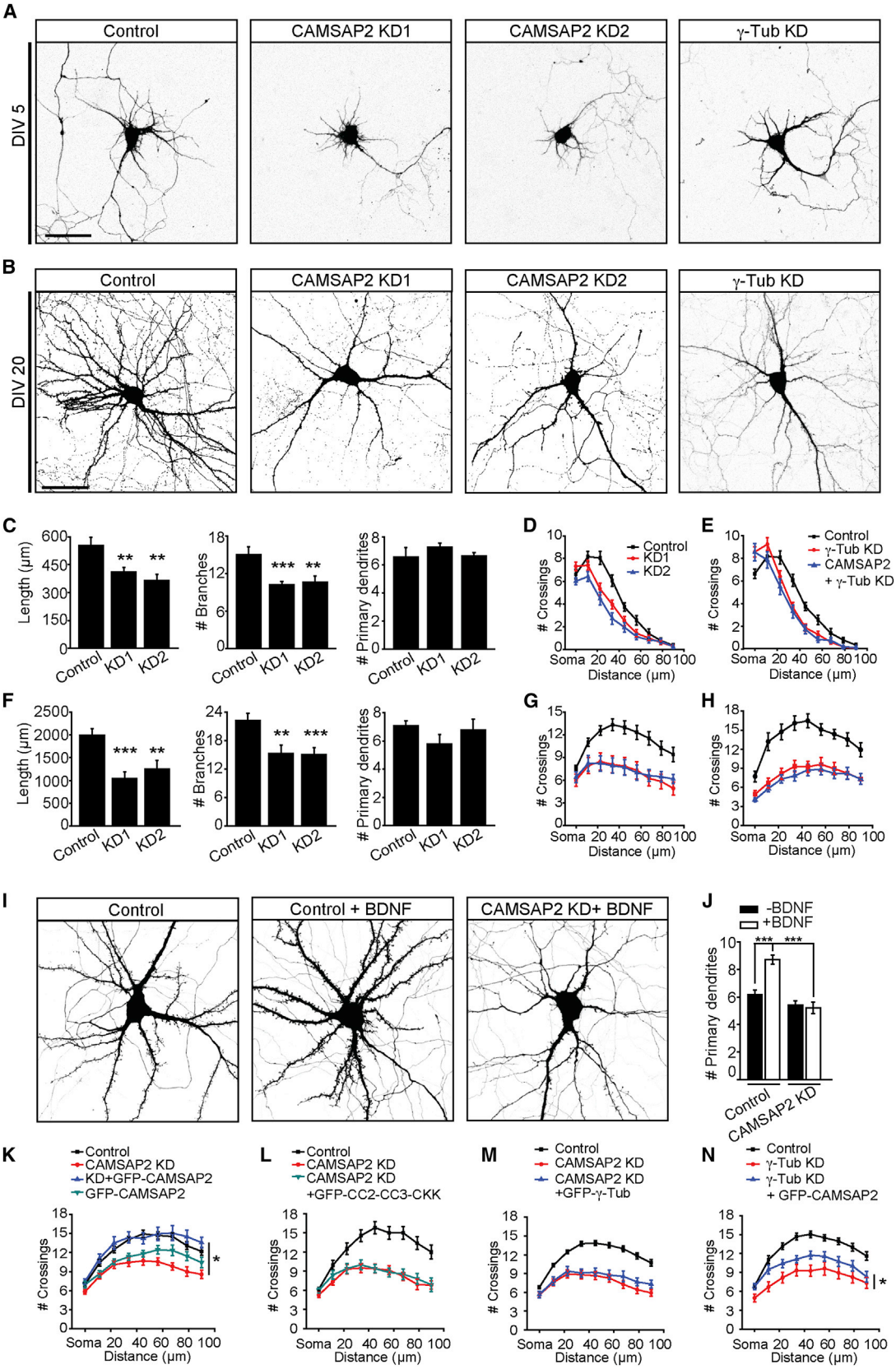

(legend on next page)

growth to generate long CAMSAP2 stretches implies that CAMSAP proteins likely act on free MT minus-ends that are not capped by γ-Tubulin or other factors. Indeed, we found that when already existing MTs are severed, CAMSAP2 is able to accumulate at the newly created MT minus-ends independently of γ-Tubulin.

CAMSAP2 is dynamic at the outmost edges of a bleached stretch, while CAMSAP2 is stably present along the length of the stretch. Once localized at the minus-ends, CAMSAP2 could act as a critical minus-end recognition signal involved in the recruitment and assembly of other factors to one specific MT end, similar to end-binding (EB) proteins at the plus-ends (Jiang et al., 2012). Our finding that the minimal CAMSAP2 minus-end binding domain (CC2-CC3-CKK) is not sufficient to restore dendrite morphology suggests that other domains and potential binding partners are involved in CAMSAP2 functions in neurons. Additional studies are required to investigate such mechanisms and for the identification of CAMSAP2 binding partners.

CAMSAP2 Is Required for Axon Specification and Neuronal Polarization

Axon formation during neuronal polarization is associated with increased MT stability (Hoogenraad and Bradke, 2009; Witte and Bradke, 2008). Here we show that neurons lacking CAMSAP2 fail to initiate axon formation and show impaired neuronal polarization during in vitro and in vivo development. The defects in neuronal migration upon CAMSAP2 depletion might be caused by the lack of polarization in the developing neocortex. Since CAMSAP2 stabilizes the neuronal MT arrays, these data suggest that noncentrosomal MT stabilization plays a critical role during the specification of axonal fate in early neuronal development. In addition, the complete block of taxol-induced axon formation in CAMSAP2-depleted neurons implies that instable MTs and subsequent decreased MT density is sufficient to block axon specification. We found that CAMSAP2 was present in the soma and small processes of neurons at early stages of neuron development (stage 2), before neuronal polarization and axon formation. In polarizing stage 3 neurons, CAMSAP2 staining is reduced at the AIS but enriched in the soma and in the proximal part of the axon, suggesting that there are no MT minus-ends in the AIS and that most MTs are continuous throughout the AIS. High levels of CAMSAP2 at the first part of the axon may create a local pool of stabilized MT minus-ends and promote plus-end out-oriented MT growth in axons. Interestingly, the increase in CAMSAP2 at the first part of the axon is maintained throughout neuronal development. Local MT stability at the site of axon formation has been reported to cause polarized membrane flow (Bradke and Dotti, 1997). Consistently, MT-based motor proteins such as kinesin-1/KIF5 show a higher affinity for stabilized MTs and have been found to transport several vesicular carriers into the axon (Kapitein and Hoogenraad, 2011). Future work will be needed to resolve the molecular interplay between CAMSAP2 and axonal transport during neuronal polarization. In addition, signaling molecules involved in the regulation of MT dynamics in axon formation and polarity processes should be reassessed for their potential role in regulating CAMSAP2 activity (Arimura and Kaibuchi, 2007).

CAMSAP2 and γ-Tubulin Are Required for Dendrite Development

We further demonstrated that CAMSAP2 stabilizes noncentrosomal MTs in dendrites. Since dendritic outgrowth occurs after the centrosome loses its function as an MTOC (Stiess et al., 2010), noncentrosomal MT assembly and stabilization is most likely an essential process during later stages of neuronal

Figure 6. CAMSAP2 Is Required for Dendrite Morphology

(A) Representative images of DIV 5 hippocampal neurons transfected at DIV 1 with mRFP and control pSuper, CAMSAP2-shRNA1 (KD1), CAMSAP2-shRNA2 (KD2) or γ-Tubulin-shRNA.

(B) Representative images of DIV 20 hippocampal neurons transfected at DIV 16 with β-galactosidase alone or with CAMSAP2-shRNA1, CAMSAP2-shRNA2, or mRFP and γ-Tubulin-shRNA. Scale bars are 50 μm.

(C) Quantification of dendrite morphology. Number of dendrites, branches, and total dendrite distance are determined from DIV 5 neurons transfected with control pSuper (n = 18), CAMSAP2-shRNA1 (n = 22) or CAMSAP2-shRNA2 (n = 17).

(D) Sholl analysis corresponding to the data used in (C).

(E) Sholl analysis of DIV 5 neurons transfected at DIV 1 with mRFP and control pSuper (n = 18), γ-Tubulin-shRNA (n = 22), or the combination of γ-Tubulin-shRNA and CAMSAP2-shRNA1(n = 17).

(F) Quantification of the number of dendrites, branches, and total dendrite distance are determined from DIV 20 neurons transfected with control pSuper (n = 25), CAMSAP2-shRNA1 (n = 13), or CAMSAP2-shRNA2 (n = 13).

(G) Sholl analysis corresponding to the data in (F).

(H) Sholl analysis of DIV 22 neurons transfected at DIV 18 with mRFP and control pSuper (n = 11), γ-Tubulin-shRNA (n = 13), or the combination of γ-Tubulin-shRNA and CAMSAP2-shRNA1 (n = 15).

(I) Representative images of DIV 22 neurons transfected with mRFP and pSuper control or CAMSAP2-shRNA1 at DIV 18 and untreated or treated with 50 ng/ml BDNF for 3 days.

(J) Quantification of the number of primary dendrites untreated (n = 28) and treated with 50 ng/ml BDNF for 3 days and transfected control pSuper (n = 50) or CAMSAP2-shRNA1 (n = 29-32 treated) at DIV 18. Neurons were fixed at DIV 22.

(K) Sholl analysis of DIV 21 neurons transfected at DIV 17 with pSuper (n = 40), CAMSAP2-shRNA (n = 30), GFP-CAMSAP2 (n = 21), or CAMSAP2-shRNA and GFP-CAMSAP2 (n = 16).

(L) Sholl analysis of DIV 21 neurons transfected at DIV17 with pSuper (n = 16), CAMSAP2-shRNA (n = 15), CAMSAP2-shRNA, and GFP-CC2-CC3-CKK (n = 15).

(M) Sholl analysis of DIV 21 neurons transfected at DIV 17 with control pSuper (n = 48), CAMSAP2-shRNA (n = 28), or CAMSAP2-shRNA1 and GFP-γ-Tubulin (n = 18).

(N) Sholl analysis of DIV 21 neurons transfected at DIV 17 with control pSuper (n = 34), γ-Tubulin-shRNA (n = 13), or γ-Tubulin-shRNA and GFP-CAMSAP2 (n = 24). Error bars represent SEM. *$p < 0.05$; **$p < 0.01$; ***$p < 0.001$ (t test).

See also Figures S5 and S6.

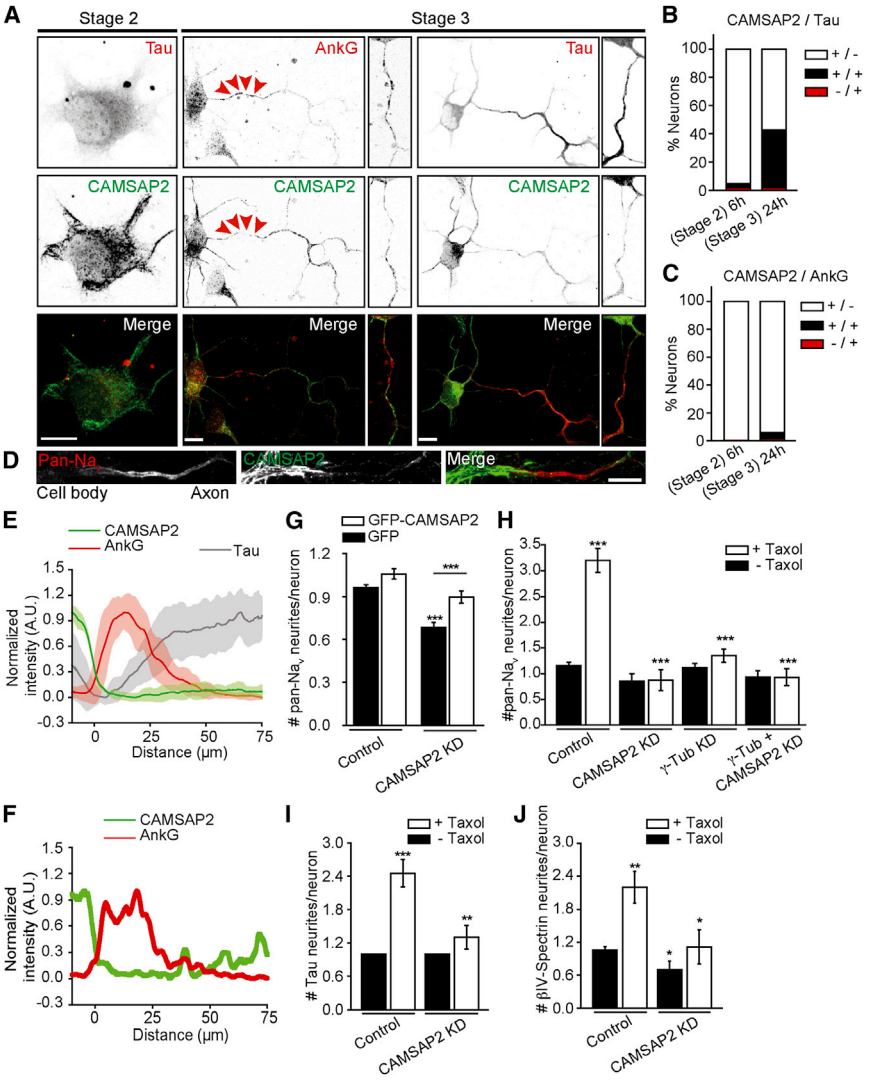

Figure 7. CAMSAP2 Is Required for Axon Formation and Neuronal Polarization

(A) Representative images of DIV 1 hippocampal neurons double stained for endogenous Tau (red) and CAMSAP2 or endogenous Ankyrin G (red) and CAMSAP2 (green). Scale bars are 10 μm.

(B) Diagram showing the percentage of neurons at DIV 0.25 and DIV 1 with neurites positive for endogenous CAMSAP2+/Tau+, CAMSAP2+/Tau−, and CAMSAP2−/Tau+ (n = 150).

(C) Diagram showing the percentage of neurons at DIV 0.25 and DIV 1 with neurites positive for endogenous Ankyrin G+/Tau+, Ankyrin G+/Tau−, and Ankyrin G−/Tau+ (n = 150).

(D) Representative image of an axonal segment from DIV 21 neuron stained for CAMSAP2 and axon initial segment marker, pan-Nav. Scale bar is 10 μm.

(E and F) Profiles of CAMSAP2 (green), Ankyrin G (red trace), and Tau (gray trace) fluorescence intensity in the axon of neurons at DIV 7. Examples of average intensity traces of at least 19 neurons for each dual staining (E) and representative single intensity traces (F). AU, arbitrary unit. Error bars represent SD.

(G) Diagram showing the number of pan-Nav-positive neurites per neuron in cortex neurons at DIV 4. Cells are electroporated before plating with pSuper control (n = 180), pSuper control and GFP-CAMSAP2 (n = 105), CAMSAP2-shRNA (n = 180), or CAMSAP2-shRNA and GFP-CAMSAP2 (n = 105) and stained for endogenous pan-Nav and CAMSAP2.

(H) Diagram showing the number of pan-Nav-positive neurites per neuron in hippocampal neurons at DIV 5; transfected at DIV 1 with mRFP and pSuper control (n = 35) or CAMSAP2-shRNA (n = 21 untreated, n = 16 treated), γ-Tubulin-shRNA (n = 17 untreated, n = 20 treated), CAMSAP2-shRNA, and γ-Tubulin-shRNA (n = 15 untreated, n = 14 treated); and untreated (n = 37) or treated with 10 nM Taxol for 48 hr.

(I and J) Diagram showing the number of Tau- or βIV-Spectrin-positive neurites per neuron in hippocampal neurons DIV 5, transfected with mRFP and pSuper control (n = 11) or CAMSAP2-shRNA (n = 10 untreated, n = 10 treated), and untreated (n = 17) or treated with 10nM Taxol for 48 hr. Error bars represent SEM. *p < 0.05; **p < 0.01; ***p < 0.001 (t test).

See also Figures S7 and S8.

development. Indeed, both stable MAP2-positive and dynamic EB3-positive MTs were reduced upon CAMSAP2 knockdown. CAMSAP2-decorated MTs were enriched in primary dendrites, consistent with the large fraction of minus-end-out MTs in this part of the dendrite (Baas et al., 1989; Stepanova et al., 2003). In the absence of CAMSAP2, dendritic branching was reduced and BDNF-induced dendrite development was inhibited. Similar to mechanisms governing neuronal polarization, we propose that dendritic branches are formed and maintained by noncentrosomal MTs that are stabilized by CAMSAP2. Our finding that γ-Tubulin knockdown also strongly reduces the MT population in dendrites suggests that many noncentrosomal MTs are generated by local nucleation. A distinct mechanism to generate noncentrosomal MTs is by severing of preexisting MTs (Bartolini and Gundersen, 2006; Kuijpers and Hoogenraad, 2011; Stiess and Bradke, 2011). Depletion of katanin and spastin has been shown to modulate axon growth in young neurons (Yu et al., 2008), but changes in dendrite outgrowth and morphology have so far not been reported. Moreover, in *Drosophila* class IV dendritic arborization neurons, mutations in the two major MT-severing proteins spastin and katanin do not induce noticeable dendrite phenotypes (Lee et al., 2009). In contrast, the complexity of the dendritic arbor in these neurons depends on the presence of Golgi outposts, which were shown to behave as MTOCs (Ori-McKenney et al., 2012). The fact that we observed a decrease in γ-Tubulin at the centrosome at early stages of development without an overall change in total protein levels suggests that similar to other systems γ-Tubulin regulates local MT nucleation throughout the neuron in a centrosome-independent manner. Therefore, we hypothesize that γ-Tubulin-dependent

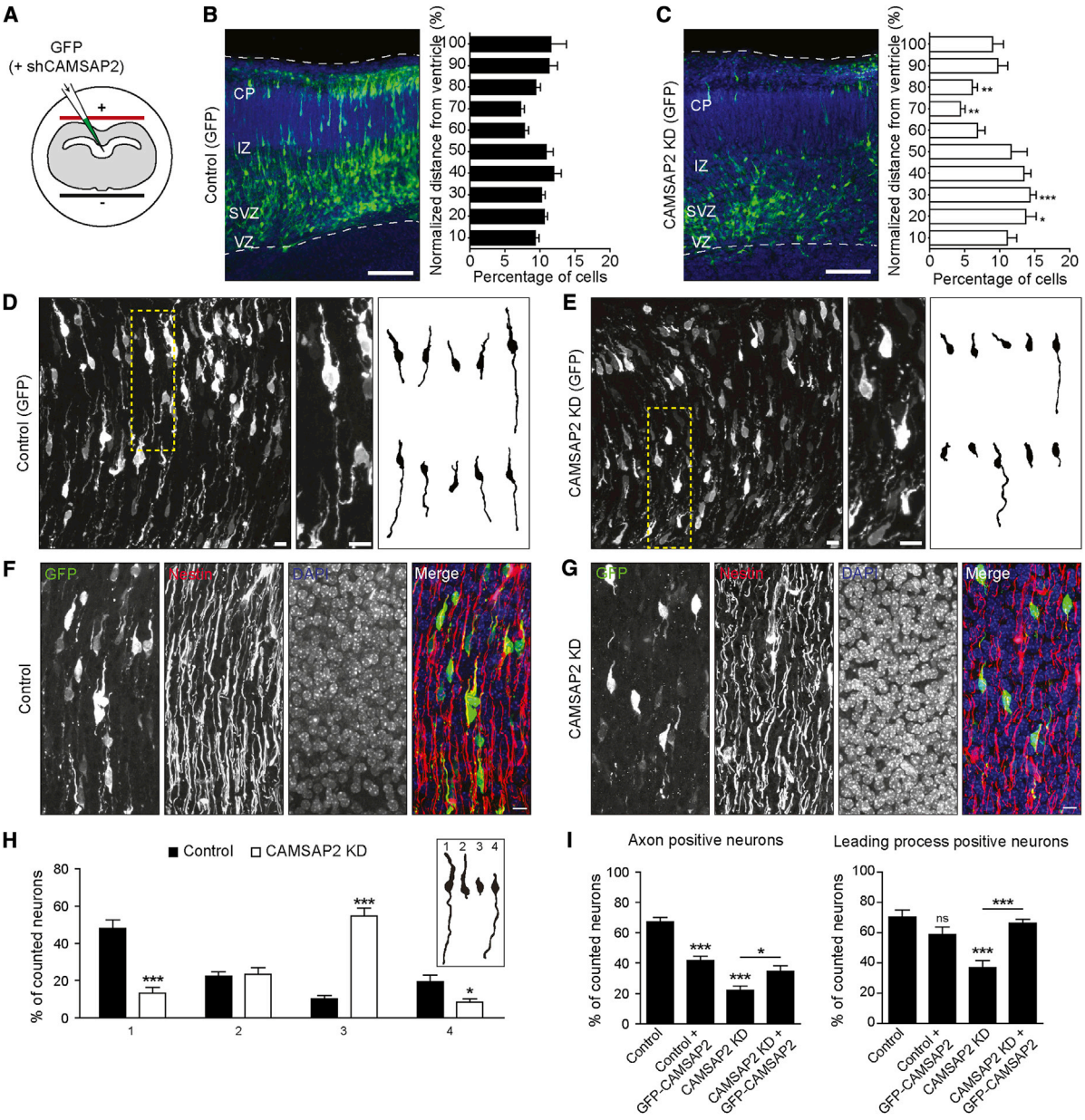

Figure 8. CAMSAP2 Is Required for Axon Initiation and Neuronal Polarity In Vivo

(A) Schematic cross section of the ex vivo electroporation procedure: E14.5 intact mouse embryo head were injected in the lateral ventricle with GFP alone or together with two CAMSAP2 shRNAs (shRNA1/2), electroporated, and followed by immediately slicing of the brains before subjecting them to organotypic slice culture for 4 days.

(B and C) Maximum intensity projection of ex vivo neuronal migration of GFP-positive neurons electroporated with either GFP only (B) or GFP and CAMSAP2 shRNAs (C). Bar diagram shows the normalized migration distribution along the radial axis from the ventricle. CP, cortical plate; IZ, intermediate zone; SVZ, subventricular zone; VZ, ventricular zone; scale bars, 100 μm; *$p < 0.05$; **$p < 0.01$; ***$p < 0.001$, comparing corresponding bins using a Mann-Whitney U Test.

(D and E) Neuron morphology (E17.5) of in utero electroporated (E14.5) mouse embryo brains. Morphology (maximum intensity projection) shown of neurons electroporated with either GFP only (D) or GFP and CAMSAP2 shRNAs (E). Middle panel contains a zoom of a typical neuron. Right panel contains individual traces of representative neurons found in the specific condition. Scale bars, 10 μm.

(F and G) Maximum intensity projection of GFP and Nestin staining (E17.5) of in utero electroporated (E14.5) mouse embryo brains. Brains were electroporated with either GFP only (F) or GFP and CAMSAP2 shRNAs (G). Scale bars are 10 μm.

(H) Quantification of the different (GFP-positive) neuronal cell morphologies found in the E17.5 brain after in utero electroporation (E14.5). *$p < 0.05$; **$p < 0.01$; ***$p < 0.001$, comparing control versus shCAMSAP2 using a Mann-Whitney U Test.

(I) Quantification of the axon-positive and GFP-positive neurons (left graph), as well as the quantification of the leading-process-positive and GFP-positive neurons (right graph) found in the E17.5 brain after in utero electroporation (E14.5). Comparing control versus control and GFP-CAMSAP2, control versus shCAMSAP2, and shCAMSAP2 versus shCAMSAP2 and GFP-CAMSAP2 using a Mann-Whitney U Test. *$p < 0.05$; **$p < 0.01$; ***$p < 0.001$.

MT nucleation and CAMSAP2-dependent stabilization are two key features of MT organization during dendritic development. We propose a two-step model in which γ-Tubulin initiates the formation of noncentrosomal MTs and CAMSAP2 subsequently stabilizes the newly formed free MT minus-ends.

In summary, we demonstrate that the CAMSAP/Nezha/Patronin family protein CAMSAP2 specifically stabilizes noncentrosomal MT minus-ends and plays an important role in the development and maintenance of neuronal structure. As changes in MT organization are important for many neuronal functions, including plasticity and regeneration, we anticipate that more neuronal processes that involve CAMSAP2 will be revealed in the future.

EXPERIMENTAL PROCEDURES

Antibodies and Reagents

The following antibodies were used in this study: rabbit anti-EB3 (02-1005-07) (Stepanova et al., 2003), mouse anti-γ-Tubulin (T6557, Sigma), rabbit anti-CAMSAP1 (Novus Biologicals, NBP1-26645), rabbit anti-CAMSAP2 (17880-1-AP, Proteintech; NBP1-21402, Novus Biologicals; HPA0273, Sigma), and rabbit anti-CAMSAP3 (Abgent, AP18323a). Details of other antibodies and reagents are in the Supplemental Experimental Procedures.

DNA Constructs

The CAMSAP2 expression constructs and their deletion mutants were generated by a PCR-based strategy using the human CAMSAP2 cDNA (IMAGE clone 40124603). The mCherry-MT+TIP construct contains the general MT + tip localization signal (SxIP motif) of human MACF2 (E5455-R5497; NP_899236) recognized by MT EB proteins. The following shRNAs were created and used in this study: γ-Tubulin-shRNA (5′-GGAGGACATCTTCAAGGAC), CAMSAP2-shRNA1, (KD1, 5′-TTGCATGTGCTCAACAGT), and CAMSAP2-shRNA2 (KD2, 5′-ATTCCAGAAGAATCGGGTG). For details see Supplemental Experimental Procedures.

Primary Hippocampal Neuron Cultures, Transfection, and Nucleofection

Primary hippocampal and cortical cultures were prepared from embryonic day 18 (E18) rat brains and transfected using Lipofectamine 2000 (Invitrogen) or the Amaxa Rat Neuron Nucleofector kit (Lonza), respectively.

Live-Cell Imaging and Laser-Induced Severing

Simultaneous dual color time-lapse live cell imaging and TIRFM was performed on a Nikon Eclipse TE2000E microscope with Coolsnap and QuantEM cameras (Roper Scientific). Neurons were maintained at 37°C with 5% CO2 (Tokai Hit). A Teem Photonics 532 nm Q-switched pulsed laser is used for laser-induced severing. The FRAP experiments were performed on a TIRF microscope system using the ILas2 system (Roper Scientific). For details see Supplemental Experimental Procedures.

Ethics Statement

All animal experiments were performed in compliance with the guidelines for the welfare of experimental animals issued by the Government of The Netherlands. All animal experiments were approved by the Animal Ethical Review Committee (DEC) of the Erasmus Medical Center and Utrecht University.

SUPPLEMENTAL INFORMATION

Supplemental Information includes eight figures, eight movies, and Supplemental Experimental Procedures and can be found with this article online at http://dx.doi.org/10.1016/j.neuron.2014.04.019.

ACKNOWLEDGMENTS

We thank Dr. Rasband for sharing βIV-Spectrin antibodies; N.T. Keijzer for cloning shRNA-constructs; Dr. F. Polleux and Dr. J. Courchet for sharing the cortical migration excel macro; and A.M.A. Chiotto for assisting with imaging and analyzing EB3 antibody stainings. This work was supported by the Netherlands Organization for Scientific Research (NWO-ALW-VICI to C.C.H. and A.A.; NWO-ALW-VIDI to L.C.K.; NWO-ALW-VENI to M.H.); the Foundation for Fundamental Research on Matter (FOM to C.C.H., L.C.K., and A.A.), which is part of the NWO; the Netherlands Organization for Health Research and Development (ZonMW-TOP to C.C.H.); the European Science Foundation (ESF-EURYI to C.C.H.); Swiss National Science Foundation (SNSF to P.S.); and European Molecular Biology Organization - Young Investigators Program (EMBO-YIP to C.C.H.).

Accepted: April 1, 2014
Published: June 4, 2014

REFERENCES

Arimura, N., and Kaibuchi, K. (2007). Neuronal polarity: from extracellular signals to intracellular mechanisms. Nat. Rev. Neurosci. *8*, 194–205.

Baas, P.W., and Lin, S. (2011). Hooks and comets: The story of microtubule polarity orientation in the neuron. Dev. Neurobiol. *71*, 403–418.

Baas, P.W., Black, M.M., and Banker, G.A. (1989). Changes in microtubule polarity orientation during the development of hippocampal neurons in culture. J. Cell Biol. *109*, 3085–3094.

Baines, A.J., Bignone, P.A., King, M.D., Maggs, A.M., Bennett, P.M., Pinder, J.C., and Phillips, G.W. (2009). The CKK domain (DUF1781) binds microtubules and defines the CAMSAP/ssp4 family of animal proteins. Mol. Biol. Evol. *26*, 2005–2014.

Barnes, A.P., and Polleux, F. (2009). Establishment of axon-dendrite polarity in developing neurons. Annu. Rev. Neurosci. *32*, 347–381.

Bartolini, F., and Gundersen, G.G. (2006). Generation of noncentrosomal microtubule arrays. J. Cell Sci. *119*, 4155–4163.

Basto, R., Lau, J., Vinogradova, T., Gardiol, A., Woods, C.G., Khodjakov, A., and Raff, J.W. (2006). Flies without centrioles. Cell *125*, 1375–1386.

Bettencourt-Dias, M., and Glover, D.M. (2007). Centrosome biogenesis and function: centrosomics brings new understanding. Nat. Rev. Mol. Cell Biol. *8*, 451–463.

Bradke, F., and Dotti, C.G. (1997). Neuronal polarity: vectorial cytoplasmic flow precedes axon formation. Neuron *19*, 1175–1186.

Cheung, Z.H., Chin, W.H., Chen, Y., Ng, Y.P., and Ip, N.Y. (2007). Cdk5 is involved in BDNF-stimulated dendritic growth in hippocampal neurons. PLoS Biol. *5*, e63.

Conde, C., and Cáceres, A. (2009). Microtubule assembly, organization and dynamics in axons and dendrites. Nat. Rev. Neurosci. *10*, 319–332.

Dammermann, A., Desai, A., and Oegema, K. (2003). The minus end in sight. Curr. Biol. *13*, R614–R624.

Efimov, A., Kharitonov, A., Efimova, N., Loncarek, J., Miller, P.M., Andreyeva, N., Gleeson, P., Galjart, N., Maia, A.R., McLeod, I.X., et al. (2007). Asymmetric CLASP-dependent nucleation of noncentrosomal microtubules at the trans-Golgi network. Dev. Cell *12*, 917–930.

Franker, M.A., and Hoogenraad, C.C. (2013). Microtubule-based transport - basic mechanisms, traffic rules and role in neurological pathogenesis. J. Cell Sci. *126*, 2319–2329.

Goodwin, S.S., and Vale, R.D. (2010). Patronin regulates the microtubule network by protecting microtubule minus ends. Cell *143*, 263–274.

Halpain, S., and Greengard, P. (1990). Activation of NMDA receptors induces rapid dephosphorylation of the cytoskeletal protein MAP2. Neuron *5*, 237–246.

Heilemann, M., van de Linde, S., Schüttpelz, M., Kasper, R., Seefeldt, B., Mukherjee, A., Tinnefeld, P., and Sauer, M. (2008). Subdiffraction-resolution fluorescence imaging with conventional fluorescent probes. Angew. Chem. Int. Ed. Engl. *47*, 6172–6176.

Hoogenraad, C.C., and Bradke, F. (2009). Control of neuronal polarity and plasticity—a renaissance for microtubules? Trends Cell Biol. *19*, 669–676.

Jaworski, J., Kapitein, L.C., Gouveia, S.M., Dortland, B.R., Wulf, P.S., Grigoriev, I., Camera, P., Spangler, S.A., Di Stefano, P., Demmers, J., et al. (2009). Dynamic microtubules regulate dendritic spine morphology and synaptic plasticity. Neuron *61*, 85–100.

Jiang, K., Toedt, G., Montenegro Gouveia, S., Davey, N.E., Hua, S., van der Vaart, B., Grigoriev, I., Larsen, J., Pedersen, L.B., Bezstarosti, K., et al. (2012). A Proteome-wide screen for mammalian SxIP motif-containing microtubule plus-end tracking proteins. Curr. Biol. *22*, 1800–1807.

Jiang, K., Hua, S., Mohan, R., Grigoriev, I., Yau, K.W., Liu, Q., Katrukha, E.A., Altelaar, A.F.M., Heck, A.J.R., Hoogenraad, C.C., and Akhmanova, A. (2014). Microtubule minus-end stabilization by polymerization-driven CAMSAP deposition. Dev. Cell *28*, 295–309.

Kapitein, L.C., and Hoogenraad, C.C. (2011). Which way to go? Cytoskeletal organization and polarized transport in neurons. Mol. Cell. Neurosci. *46*, 9–20.

Kapitein, L.C., Yau, K.W., Gouveia, S.M., van der Zwan, W.A., Wulf, P.S., Keijzer, N., Demmers, J., Jaworski, J., Akhmanova, A., and Hoogenraad, C.C. (2011). NMDA receptor activation suppresses microtubule growth and spine entry. J. Neurosci. *31*, 8194–8209.

Kuijpers, M., and Hoogenraad, C.C. (2011). Centrosomes, microtubules and neuronal development. Mol. Cell. Neurosci. *48*, 349–358.

Lee, H.H., Jan, L.Y., and Jan, Y.N. (2009). Drosophila IKK-related kinase Ik2 and Katanin p60-like 1 regulate dendrite pruning of sensory neuron during metamorphosis. Proc. Natl. Acad. Sci. USA *106*, 6363–6368.

Meng, W., Mushika, Y., Ichii, T., and Takeichi, M. (2008). Anchorage of microtubule minus ends to adherens junctions regulates epithelial cell-cell contacts. Cell *135*, 948–959.

Millecamps, S., and Julien, J.P. (2013). Axonal transport deficits and neurodegenerative diseases. Nat. Rev. Neurosci. *14*, 161–176.

Nguyen, M.M., Stone, M.C., and Rolls, M.M. (2011). Microtubules are organized independently of the centrosome in *Drosophila* neurons. Neural Dev. *6*, 38.

Ori-McKenney, K.M., Jan, L.Y., and Jan, Y.N. (2012). Golgi outposts shape dendrite morphology by functioning as sites of acentrosomal microtubule nucleation in neurons. Neuron *76*, 921–930.

Rust, M.J., Bates, M., and Zhuang, X. (2006). Sub-diffraction-limit imaging by stochastic optical reconstruction microscopy (STORM). Nat. Methods *3*, 793–795.

Stepanova, T., Slemmer, J., Hoogenraad, C.C., Lansbergen, G., Dortland, B., De Zeeuw, C.I., Grosveld, F., van Cappellen, G., Akhmanova, A., and Galjart, N. (2003). Visualization of microtubule growth in cultured neurons via the use of EB3-GFP (end-binding protein 3-green fluorescent protein). J. Neurosci. *23*, 2655–2664.

Stiess, M., and Bradke, F. (2011). Neuronal polarization: the cytoskeleton leads the way. Dev. Neurobiol. *71*, 430–444.

Stiess, M., Maghelli, N., Kapitein, L.C., Gomis-Rüth, S., Wilsch-Bräuninger, M., Hoogenraad, C.C., Tolić-Nørrelykke, I.M., and Bradke, F. (2010). Axon extension occurs independently of centrosomal microtubule nucleation. Science *327*, 704–707.

Tanaka, N., Meng, W., Nagae, S., and Takeichi, M. (2012). Nezha/CAMSAP3 and CAMSAP2 cooperate in epithelial-specific organization of noncentrosomal microtubules. Proc. Natl. Acad. Sci. USA *109*, 20029–20034.

Witte, H., and Bradke, F. (2008). The role of the cytoskeleton during neuronal polarization. Curr. Opin. Neurobiol. *18*, 479–487.

Witte, H., Neukirchen, D., and Bradke, F. (2008). Microtubule stabilization specifies initial neuronal polarization. J. Cell Biol. *180*, 619–632.

Yu, W., Qiang, L., Solowska, J.M., Karabay, A., Korulu, S., and Baas, P.W. (2008). The microtubule-severing proteins spastin and katanin participate differently in the formation of axonal branches. Mol. Biol. Cell *19*, 1485–1498.